

Properties of Aqueous Solutions of Polyelectrolytes and Surfactants of Opposite Charge: Surface Tension, Surface Rheology, and Electrical Birefringence Studies

H. Ritacco, D. Kurlat, and D. Langevin*

Laboratorio de Sistemas Líquidos, Facultad de Ingeniería, Paseo Colon, Buenos Aires, Argentina

Received: January 7, 2003

We describe the dynamic behavior of both surface and bulk of mixed aqueous solutions of surfactants and polymers of opposite electrical charges. We evidence the importance of the point of equivalence of charges (EP), which occurs well before precipitation in our systems. Close to EP, an adsorption barrier, possibly due to charge reversal, starts to build up at the surface. In the bulk, the surfactant not only screens the polymer charges but is likely to start binding to the polymer chains.

Introduction

Interactions of surfactants and polymers in aqueous solvents is a very active research area.^{1,2} Indeed, this topic poses interesting fundamental problems, quite different from those of either pure surfactants or pure polymers, in view of the large number of possible regimes due to the interactions. The behavior is especially rich when the surfactant and the polymer bear opposite electrical charges; it is also usually very different than that for polymers and simple salts, suggesting that interactions other than electrostatic (hydrophobic, hydration, etc.) play important roles. The mixed solutions are used in many practical applications because they are the basis of industrial formulations in which surfactants are used as detergents or dispersing and wetting agents and polymers are used as thickening agents.

In the present paper, we describe studies of aqueous solutions of a cationic surfactant, dodecyltrimethylammonium bromide (DTAB), and an anionic polymer, a sulfonated polyacrylamide (PAMPS). Previous surface tension studies³ showed that surfactant–polymer complexes start to form at very low surfactant concentration, more than an order of magnitude below the critical micellar concentration (CMC). Above a critical aggregation concentration (CAC), the surface tension exhibits a plateau region, and the CAC was assumed to signal the onset of formation of bulk aggregates, as in former studies.¹ Recent measurements with electrodes specific to surfactant ions showed however that surfactant starts to bind to the polymer already below the CAC.⁴ Previous studies of the surface of the solution also included ellipsometry,⁵ X-ray reflectivity (to determine the thickness of the mixed surface layers),^{6,7} and capillary waves (to determine the surface rheology).⁸ The bulk properties were investigated by viscosimetry.³ The picture that emerges is that the surface layer becomes more compact as one approaches the CAC, after which the polymer becomes progressively less surface-active and also forms complexes with surfactant in the bulk. When the surfactant concentration is small, the polymer chains are extended because of the electrostatic repulsion and form a network with overlap points (entanglements are formed only at large concentrations, when sufficient self-screening of electrostatic repulsion is present; here the viscosity of the solution is small enough and no entanglements are present).

Around CAC, the polymer chains start to progressively collapse, and when the precipitation limit is approached, the bulk aggregates grow and become very large.⁹

In this paper, we present complementary investigations of the surface properties. We also present bulk experiments done with a technique more sensitive to the local chain properties, electrical birefringence. Earlier measurements done on polyelectrolyte solutions showed that the method is particularly sensitive to the local environment of the chains, to the presence of overlap points in the semidilute regime, for instance.^{10,11} It was therefore tempting to investigate the mixed solutions with this technique.

1. Materials

PAMPS is an anionic statistical copolymer of neutral acrylamide monomers and charged monomers of acrylamido methyl propane sulfonate (PAMPS). In this work, we use a polymer with a degree of charge of 25% (ratio of number of sulfonated monomers to the total number of monomers) that we will call PAMPS25%, as in earlier studies.³ This value is close to the maximum number of effective charges that the polymer chain can bear; indeed, due to Manning condensation, there cannot be more than one effective charge per Bjerrum length (0.7 nm at room temperature); with a monomer length on the order of 0.25 nm, $f_{\max} \approx 30\%$.¹² The polymer was synthesized by SNF Floerger, dissolved in deionized water, and purified with an ultrafiltration unit with a 20 000 Da cutoff membrane. It was provided to us by the Institut Français du Pétrole. The polymer molecular weight, the mean monomer molecular weight, and the polymerization degree are $M_w \approx 4 \times 10^5$ g/mol, $M_{\text{monomer}} \approx 100$, and $N \approx 4000$, respectively.

The surfactant is dodecyl trimethyl ammonium bromide (DTAB), which was supplied by SIGMA and used without further purification (>99% purity).

Deionized water was from a DEIONEX MS 160 equipment, its resistivity being 12 M Ω .

All of the measurements are performed at $T = 298 \pm 0.5$ K unless stated otherwise. The solutions were prepared from concentrated stock solutions of polymer and surfactant, which were diluted and mixed.

The experiments with mixed solutions were done 7 days after the preparation. All solutions were kept in a refrigerator between measurements and were discarded after 1 month.

* To whom correspondence should be addressed. Present address: Laboratoire de Physique des Solides, Université Paris Sud, 91405 Orsay, France.

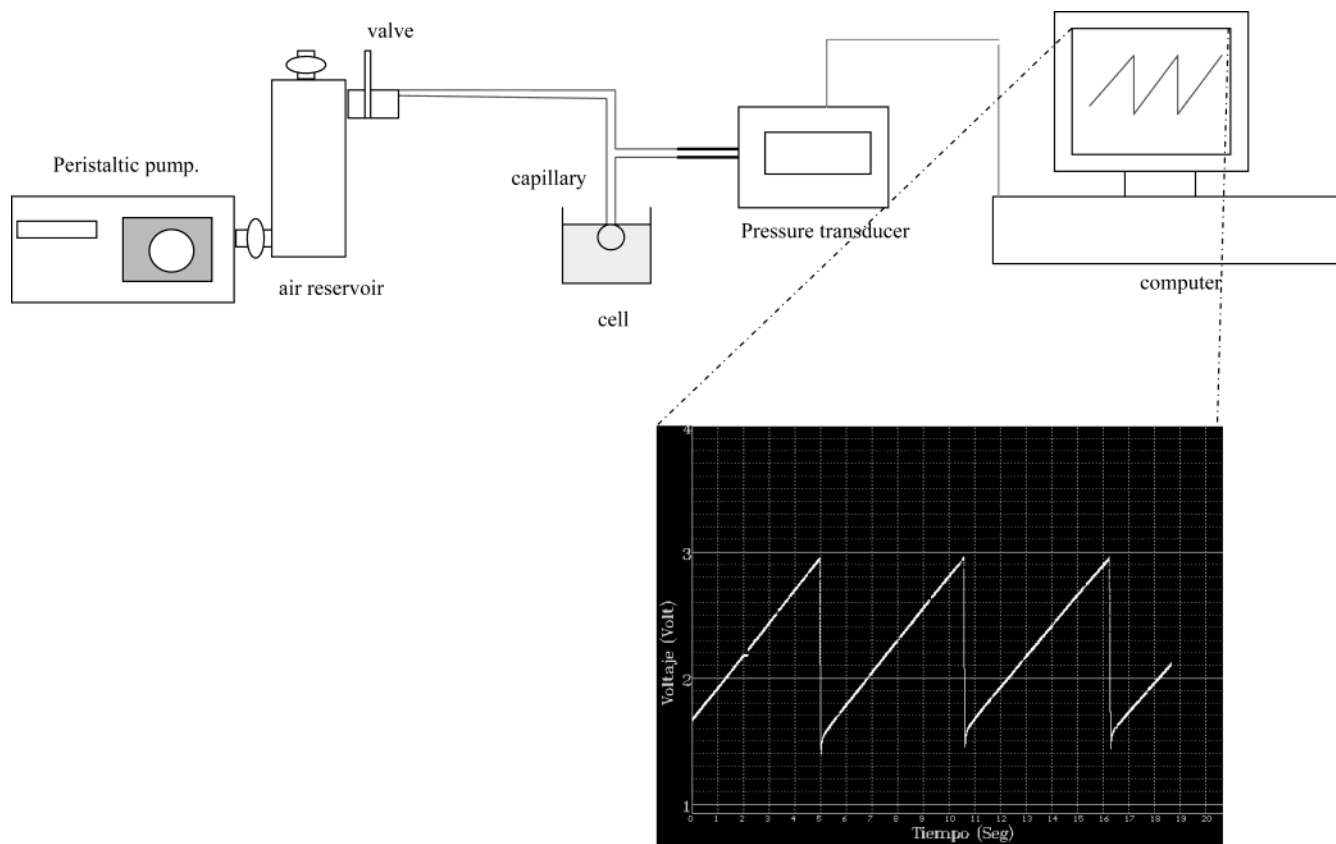


Figure 1. Schematic representation of the maximum bubble pressure instrument.

2. Methods

2.1. Surface Tension. The surface tension of the solutions was measured with different methods: Wilhelmy plate,³ maximum bubble pressure, and pendant drop methods described below. In this work, we investigated more particularly the “dynamic” surface tension, that is, the time variation of the surface tension before it reaches equilibrium.

2.2. Dynamic Surface Tension. *2.2.1. Maximum Bubble Pressure Method.* The dynamic surface tension was measured by means of an equipment designed and made in our laboratory (Figure 1). This equipment uses the maximum bubble pressure technique (MBP). This method involves measuring the maximum pressure necessary to detach a bubble in a liquid from the tip of a capillary. The surface tension can then be determined from the Young–Laplace equation:

$$\Delta P = \gamma \left(\frac{1}{R_1} + \frac{1}{R_2} \right) \quad (1)$$

where γ is the surface tension, ΔP is the pressure difference between the gas in the bubble and the liquid, and R_1 and R_2 are the two principal radii of curvature. For a spherical interface,

$$\gamma = \frac{\Delta P R}{2}$$

where R is the radius of the bubble.

The equipment makes use of a glass capillary of a 0.213 mm internal radius. The capillary is plunged into the solution, the tip being situated 2 mm away from the surface. The pressure is generated by means of a peristaltic pump connected to a 250 cm³ air reservoir to damp the external pressure fluctuations (and to increase the total volume of the system). This reservoir is connected to a valve that controls the air flow to the capillary.

The pressure difference between the inner and outer sides of the bubble is measured by means of a pressure transducer (maximum pressure = 25 cm H₂O, accuracy = 1% of the maximum pressure) connected to a computer. This experimental setup allows the measurement of the dynamic surface tension of surfaces the ages of which are greater than or equal to 0.05 s.

The solution is filled in a 40 mL closed glass container, placed in a chamber that is temperature-controlled via water circulation (± 0.2 °C).

In this technique, the surface is growing continuously. So, the surface age is less than the time elapsed between bubble formation and detachment.^{13,14} If convection is neglected and if one assumes that the adsorption kinetics is controlled by diffusion of the surface active species from bulk to surface, one can use the classical Ward and Tordai's equation for a radially symmetric bubble growing at constant rate:¹³

$$\Gamma = 2C_b \sqrt{\frac{3Dt}{7\pi}} - 2\sqrt{\frac{D}{\pi}} t^{-2/3} \int_0^{\sqrt{t}} C_b(t-\lambda) d(\sqrt{\lambda}) \quad (2)$$

where Γ is the surface concentration, t is the bubble lifetime (time between formation and detachment), and λ is a dummy variable.

Equation 2 can be solved at either short times or long times (close to equilibrium). Here, in view of the concentrations used, we will essentially measure long-time limits, as far as diffusion is concerned. The long-time limit for nonionic surfactants or ionics in the presence of an excess of non-surface-active electrolyte surfactants is¹⁵

$$\gamma = \gamma_{eq} + \frac{2RT\Gamma^2}{C_b} \sqrt{\frac{7\pi}{12Dt}} \quad (3)$$

For ionic surfactants, a factor 2 needs to be introduced (RT replaced by $2RT$). From this expression, one sees that at long times, the surface tension is proportional to $t^{-1/2}$ when adsorption is diffusion-controlled.

The instrument was tested with Triton X-100 aqueous solutions. The surface-tension variations with time are in good agreement with literature values for the MBP technique, even for times slightly less than seconds, showing that uncontrolled convection effects are negligible in our experiments.

2.2.2. The Pendant Drop Method. In this method, the shapes of drops or bubbles are recorded and analyzed. We have used a commercial instrument (IT Concept, Longessaigne, France):¹⁶ A bubble is formed at the end of a needle in a quartz cell containing the solution. A light source illuminates the bubble uniformly. The bubble is imaged by an objective onto a CCD camera (512 pixels \times 512 pixels) and the image is digitized.

The shape of the bubble is determined by surface tension and gravity forces. The balance between them is reflected in the Laplace equation, which is the mechanical equilibrium condition for two homogeneous fluids separated by an interface (eq 1). The pressure difference between the gas in the bubble and the liquid, ΔP , may be written as

$$\Delta P = \Delta P_0 + \Delta \rho g z \quad (4)$$

where ΔP_0 is the pressure difference at a reference height, $\Delta \rho$ is the density difference between the two phases, g is the gravitational acceleration, and z is the vertical height of the bubble measured from the reference. With this equation, it is possible to determine the surface tension from the shape of a bubble (or drop). In the case of axisymmetric drops or bubbles, numerical procedures can be devised. The software of the instrument allows one to measure the time variation of the bubble surface, bubble volume, and surface tension.

The surface tensions measured with this apparatus were not very reproducible with our solutions (although very good results were obtained with other systems, pure surfactant solutions, protein solutions, etc.). We do not know what is the origin of the problems with the systems used in this work. However, the results obtained for the surface elasticity with oscillating bubbles were very reproducible. We will therefore only present these results here.

2.3. Surface Rheology: The Oscillating Bubble Method.

The pendant drop instrument allows one to perform periodic variations of the bubble volume or area, for example, sinusoidal. The surface tension becomes then a sinusoidal function of time with the same frequency. If ΔA is the amplitude of the area change and $\Delta \gamma$ the amplitude of the surface tension change, the surface dilational elasticity is given by

$$\epsilon = A \frac{\Delta \gamma}{\Delta A} \quad (5)$$

From the phase shift between surface area and tension variation θ , the real and imaginary parts of the elastic modulus can be obtained: $\epsilon_r = \epsilon \cos \theta$, and $\epsilon_i = \epsilon \sin \theta$.¹⁶

2.4. Electrical Birefringence: Kerr Effect. We have also studied the bulk properties of the solution by using the electrical birefringence method also called Kerr effect. The birefringence is defined as

$$\Delta n = n_{\parallel} - n_{\perp} \quad (6)$$

where n_{\parallel} and n_{\perp} are the refraction indices in the directions parallel and perpendicular to the applied electric field, respec-

tively. In the case of an isotropic system, such as a liquid, when there is no field, the birefringence is null.

To measure the Kerr effect, we have used a homemade equipment.¹⁷ A polarized laser light beam ($\lambda = 632.8$ nm) is sent through two crossed crystal polarizers (coined as "polarizer" and "analyzer", respectively). The sample is placed into a quartz cuvette (Hellma Q-S -500; $L = 50$ mm) containing two electrodes, which are stainless steel plain parallel plates at a distance of 2 mm. These electrodes are connected to a high-voltage source ($100 \text{ V} < E < 2.5 \text{ kV}$), which generates square pulses (rise/decay time < 100 ns, minimum width $10 \mu\text{s}$). In the experiments described here, the width of the pulses was chosen equal to $225 \mu\text{s}$ to avoid heating of the samples. The polarizer and analyzer principal axes are set at an angle α . A quarter wave plate making an angle of 135° with respect to the applied field electric direction is placed between polarizer and analyzer. This device allows one to measure the sign of the birefringence.

In most liquids, the induced birefringence is a linear function of E^2 :

$$\Delta n = BE^2 \quad (7)$$

B is called the Kerr constant.

This type of behavior (Kerr regime) was found for all of the systems studied here. The B values are obtained from the slope of the Δn vs E^2 lines.

The transient regimes, after the electric field rise or decay, can also be analyzed. Typical curves are shown in Figure 2. The relaxation curves were fitted with exponential curves leading to relaxation times τ .

2.5. Viscosity. For viscosity measurements, we have used a rolling ball viscosimeter set up, which was developed in our laboratory. This technique is based on the measurement of the time that a rolling ball takes to travel a fixed distance into a glass pipe filled with the liquid. The angle (α) made by the pipe and the horizontal is 10° , 20° , or 30° . Measured viscosities were not observed to depend on α . The final value is taken as the mean value of the measurements for all angles. The accuracy is on the order of 3%.

3. Experimental Results and Discussion

3.1. Surface Tension. The measured equilibrium surface tensions of the PAMPS(25%)/DTAB (Figure 3) are in agreement with those of ref 3, made at a higher polymer concentration (750 ppm). The CAC plateau begins at a DTAB concentration close to 0.7 mM. The surface tension curves, as well as the CAC, are independent of the polymer concentration, as expected.³

3.2. Dynamic Surface Tension Results. Examples of dynamic surface tension variation curves are shown in Figure 4. Above the equivalent point of charges (EP), defined as the concentration at which the DTAB concentration is equal to the concentration of charged groups on the polyion, an unexpected behavior is observed: the two regions are separated by a plateau region (Figure 4b). In previous studies,⁷ the time resolution was not as good as that with the MBP, and these plateaus, which are found in the first seconds in these systems, were not evidenced. At still larger concentrations, oscillations can be seen when the polymer concentration is large (Figure 4c). Close to CMC, the curves depend on the rate of pressure change (Figure 4d). In Figure 5, the data of Figure 4b are represented as a function of $t^{-1/2}$. Two regions are seen with different slopes. This could be due to the adsorption of two different species of

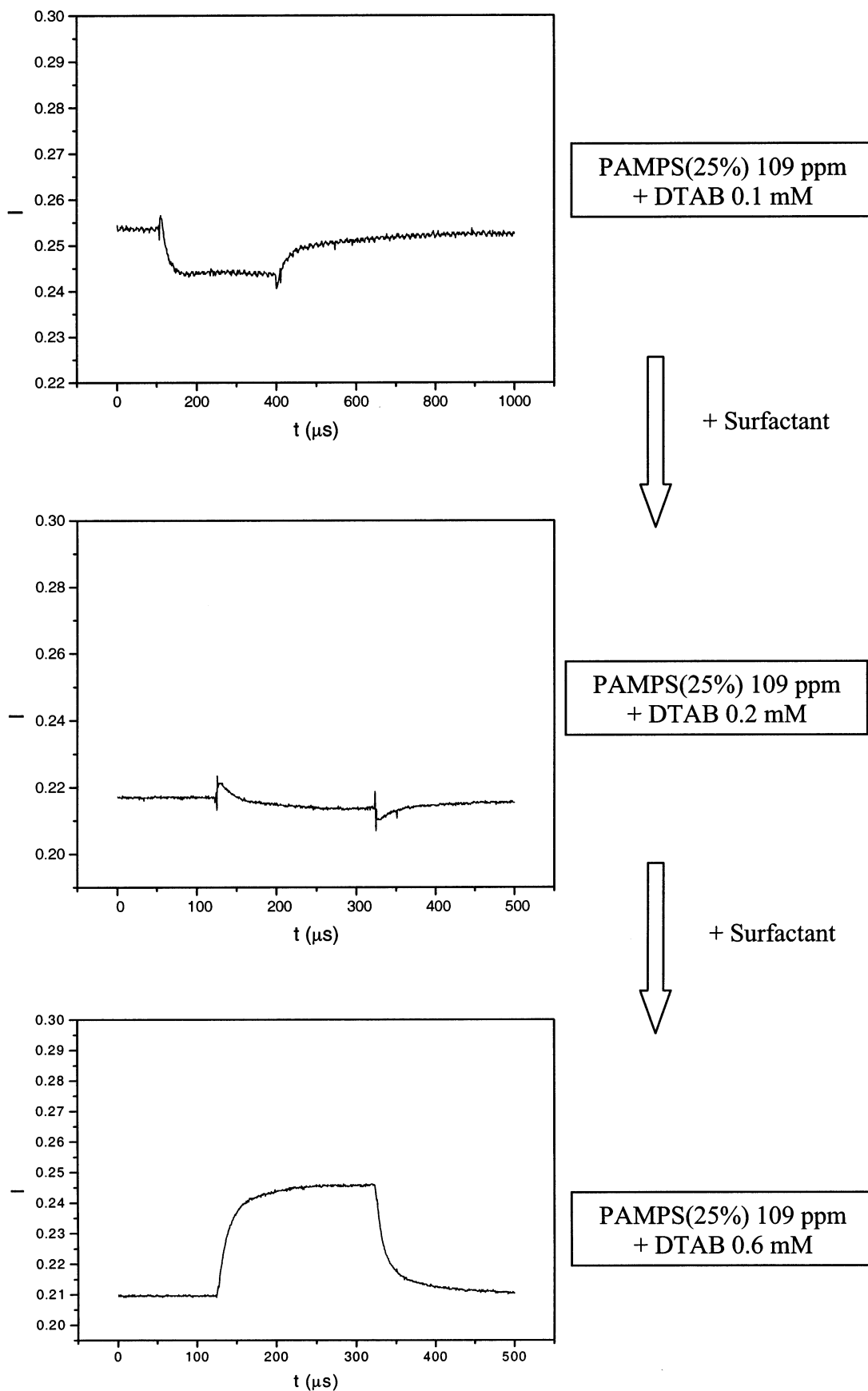


Figure 2. Typical transient Kerr signals for solutions containing 109 ppm polymer and various surfactant concentrations: (a) $C_S = 0.1$ mM (negative B); (b) $C_S = 0.2$ mM ($B \approx 0$); (c) $C_S = 0.6$ mM (positive B). Voltage is 1300 V.

different concentration or sizes. Similar plots were observed for all curves (except those like Figure 4d), oscillations and

plateaus being smoothed out in this kind of representation. The long-time limit was the limit studied in the previous work.⁷

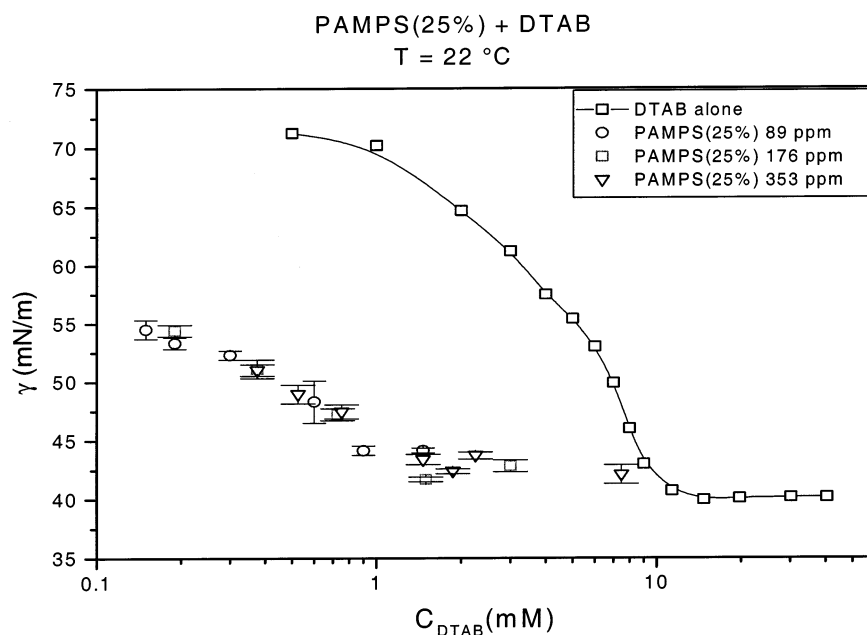


Figure 3. Equilibrium surface tension for PAMPS/DTAB systems.

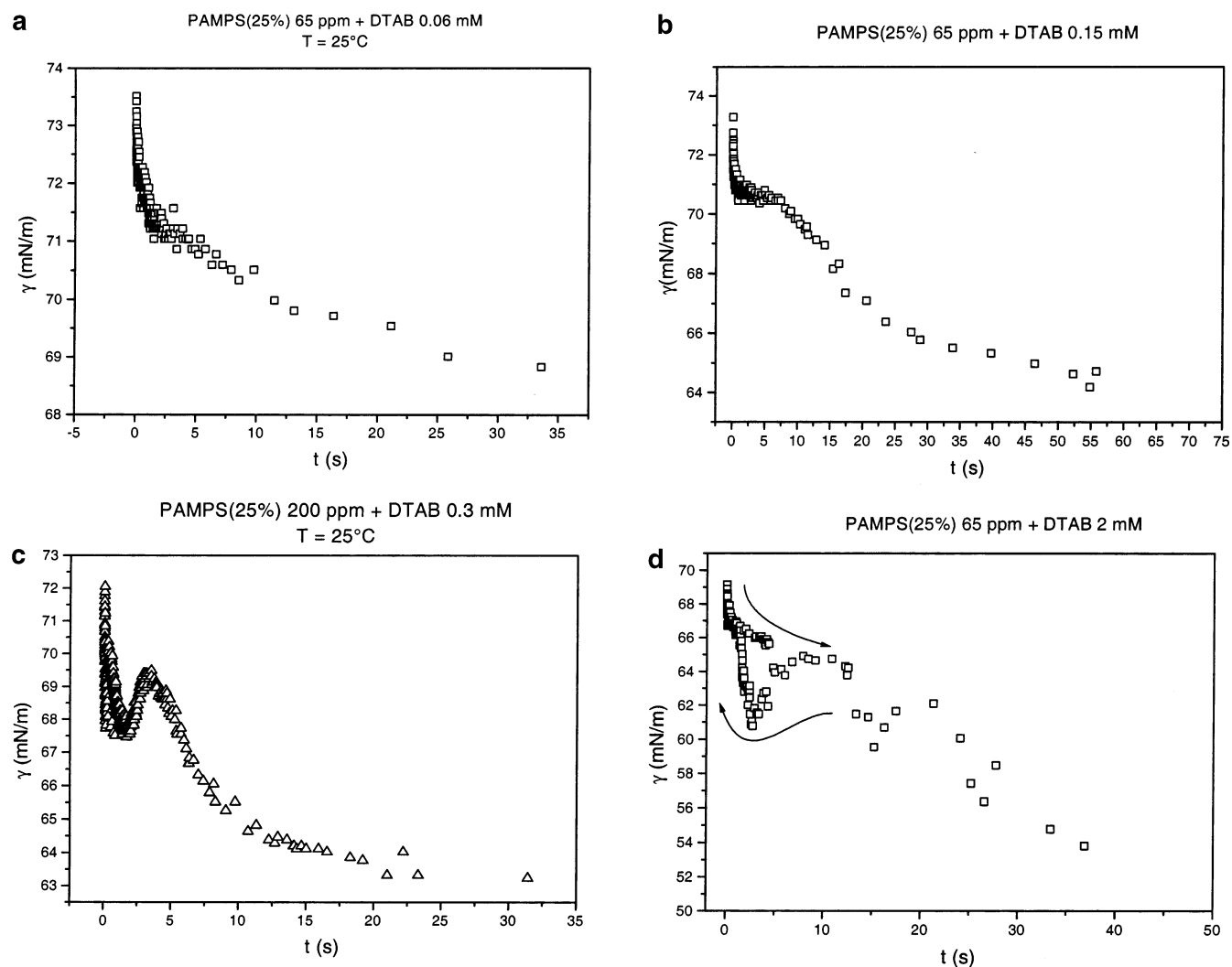


Figure 4. Typical dynamic surface tension curves: (a) $C_P = 65$ ppm, $C_S = 0.06$ mM; (b) $C_P = 65$ ppm, $C_S = 0.15$ mM; (c) $C_P = 200$ ppm, $C_S = 0.4$ mM (d) $C_P = 65$ ppm, $C_S = 2$ mM.

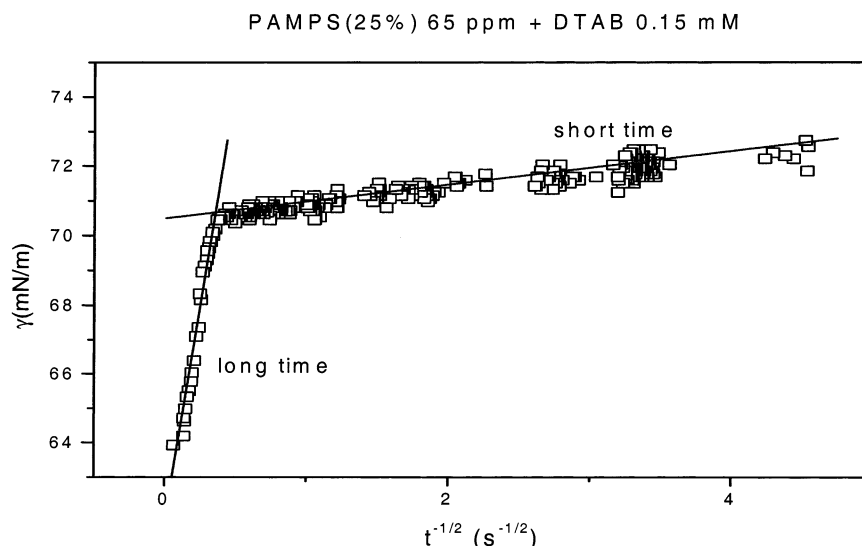


Figure 5. Typical dynamic surface tension curve, $\gamma(t^{-1/2})$ representation.

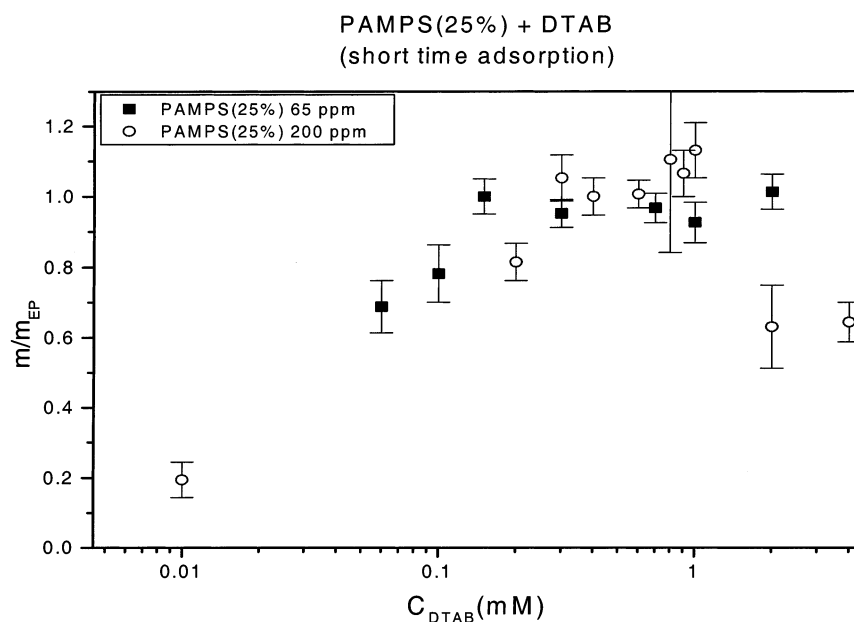


Figure 6. Slopes, m , of short-time behavior for two different polymer concentrations versus surfactant concentration: $m_{EP} = 0.47 \text{ mN m}^{-1} \text{ s}^{1/2}$ (for $C_P = 65 \text{ ppm}$); $m_{EP} = 1.52 \text{ mN m}^{-1} \text{ s}^{1/2}$ (for $C_P = 200 \text{ ppm}$).

Let us first discuss the short-time adsorption limit.

3.2.1. Short-Time Limit. In the following, we will call m the slopes of the curves $\gamma(t^{-1/2})$. Figure 6 shows their relative variation as a function of DTAB concentration system. Here, the slope m levels around the EP; indeed, the calculated EP is 0.4 mM for 200 ppm PAMPS and 0.13 mM for 65 ppm. At concentrations above EP, m remains approximately constant up to 2 mM, after which the solutions become cloudy and the measurements less-reliable.

The plateau region of the $\gamma(t)$ curves (Figure 4b) is really visible above the EP; its range increases with DTAB concentration, until it disappears above CAC. The dynamic surface tension curves then adopt complicated shapes (Figure 4c,d). The origin of this peculiar behavior might be associated with adsorption/desorption of bulk aggregates sticking to the surface layers as evidenced earlier with ellipsometry.⁵

3.2.2. Long-Time Limit. The relative variation of m with DTAB concentration is shown in Figure 7. We see that m increases with DTAB concentration up to concentrations

between 0.7 and 1 mM. This concentration is very close to the CAC. At DTAB concentrations close to 2 mM, the system becomes cloudy and m does not change appreciably (in view of the large error bars). This variation and the characteristic time scales are in agreement with those of previous studies.⁷

3.3. Surface Viscoelasticity. In Figure 8a,b, we show the real and imaginary parts of the elasticity modulus for different polymer concentrations at a frequency of 0.05 s^{-1} . Measurements were also made at 0.1 s^{-1} , and the results are identical within error bars. As seen in Figure 8, the moduli do not depend on polymer concentration either. A maximum is seen at DTAB concentrations between 0.3 and 0.6 mM for both ϵ_r and ϵ_i . This is close to the CAC and may indicate that at this point the mixed surface layer has a maximum density.

Earlier results obtained at higher frequency (200–800 Hz) with excited capillary waves methods are very similar.⁸ The numerical values of ϵ_i are even close in the region of the maximum. This is somewhat surprising, because ϵ_i is associated

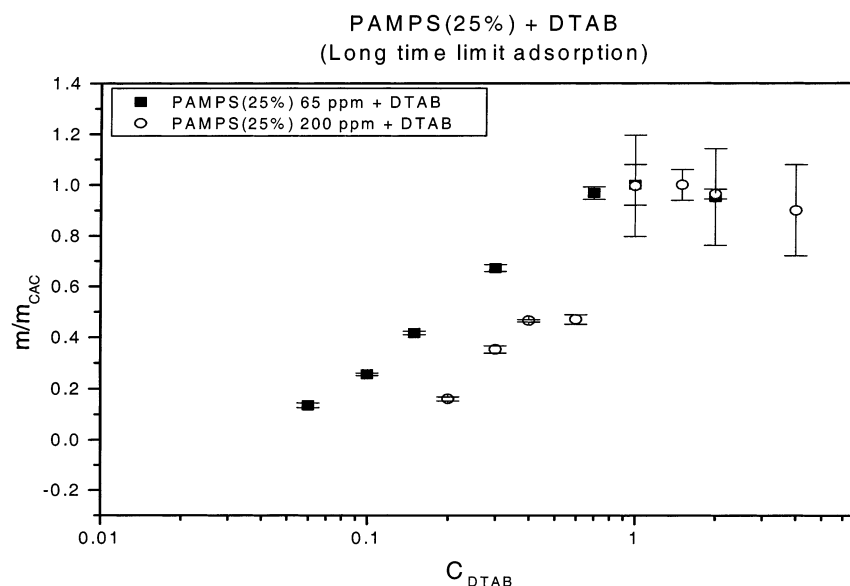


Figure 7. Slopes, m , of long-time behavior for two different polymer concentrations versus surfactant concentration: $m_{CAC} = 70 \text{ mN m}^{-1} \text{ s}^{1/2}$ (for $C_P = 65 \text{ ppm}$); $m_{CAC} = 62 \text{ mN m}^{-1} \text{ s}^{1/2}$ (for $C_P = 200 \text{ ppm}$).

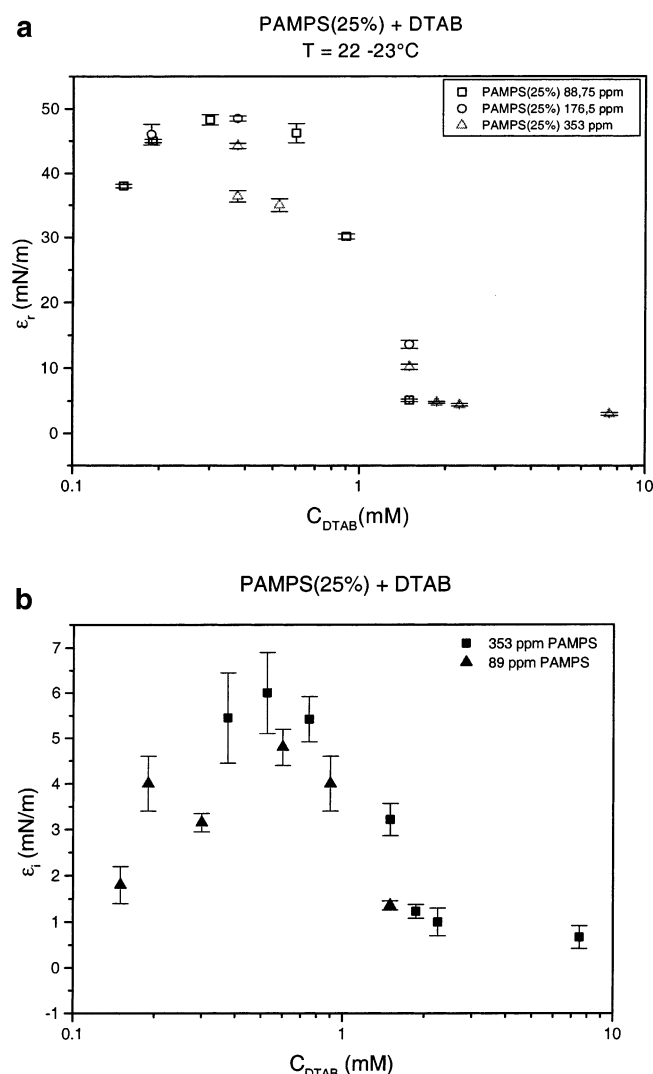


Figure 8. Elastic compression modulus versus surfactant concentration for different polymer concentrations at a frequency of 0.05 s^{-1} : (a) real part; (b) imaginary part.

with surface relaxation times and should be frequency-dependent. It should be stressed however that the oscillating drop data

should be considered with caution, because of the unreliable behavior of the surface tension in these systems as quoted earlier. Furthermore, the values of ϵ_r are about twice larger at low frequencies than at high frequencies, an unphysical behavior. It can therefore only be said that the behavior is qualitatively similar at all frequencies.

3.4. Kerr Effect. In all cases, we found a “Kerr behavior”, that is, a birefringence that varies linearly with E^2 ; we could also fit the relaxations with single exponentials and derive a relaxation time τ . Figure 9a,b shows the Kerr constant and the relaxation times for solutions containing only polymer. The Kerr constant is negative for all of the solutions studied, whereas that of pure water is positive. This is similar to earlier results.^{10,11} The absolute value of the Kerr constant exhibits a maximum around 200 ppm, which might indicate the region where the solutions enter the semidilute range. The relaxation time is significantly larger than that for water, but surprisingly, it does not change with polymer concentration (for $c > 65 \text{ ppm}$), although the bulk viscosity does. This suggests that the electrical birefringence is sensitive to very local processes in the chains.

Figure 10 shows the variation of the Kerr constant with surfactant concentration. For the sake of comparison, experiments with samples in which salt has been used instead of surfactant are also shown on the figure. There are striking differences between the two curves: when salt is added, the Kerr constant decreases in absolute value and tends toward the water value at high salt concentration ($B_{\text{water}} = 3.2 \times 10^{-14} \text{ m V}^{-2}$). This is as found earlier^{10,11} and is due to the electrostatic screening of the charges on the polymer chain. When surfactant is added, only the behavior at low concentrations is similar. The Kerr constant vanishes at approximately the point of zero charge (EP = 0.13 mM), and then exhibits a maximum close to the CAC, after which it decreases toward the water value. Experiments were not possible after 2 mM surfactant because of the turbidity of the solutions.

Results for DTAB without polymer are also shown in the figure. In this case, the Kerr constant is small and constant up to around the CMC.

Experiments done at higher polymer concentrations were qualitatively similar, as shown in Figure 11. The concentrations at which B vanishes are different, and all are near the EP. The

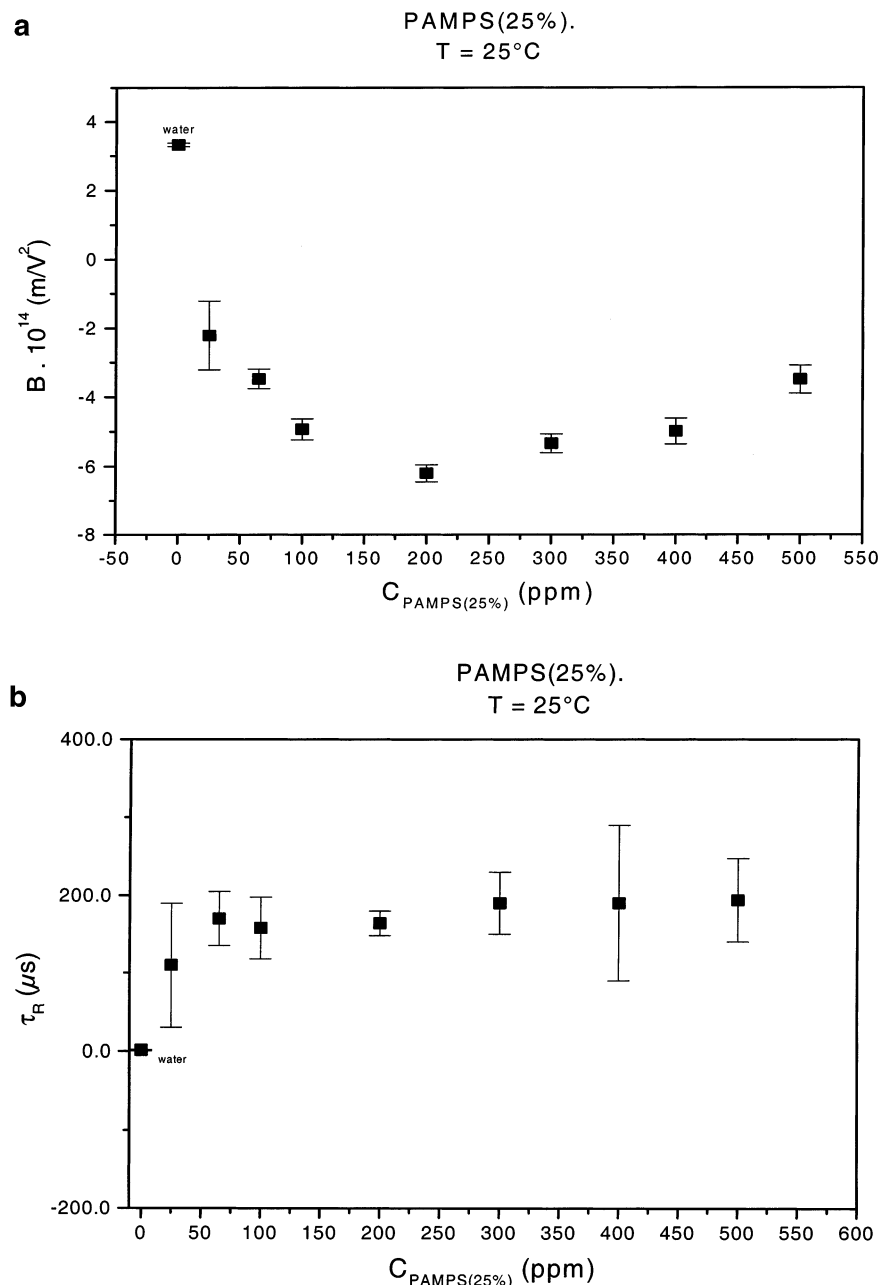


Figure 9. Electrical birefringence of pure polymer solutions versus polymer concentration: (a) Kerr constant; (b) relaxation time.

maximum value of the Kerr constant is somewhat larger for the largest investigated polymer concentration, but the maxima are all close to CAC. The relaxation times strongly decrease when surfactant is added (Figure 12).¹⁸ A shallow maximum is however observed close to the CAC.

3.5. Bulk Viscosity. Bulk viscosities measured for two different polymer concentrations are shown in Figure 13. At low surfactant concentrations, the viscosity is high because the chains are overlapping (semidilute solutions). At larger surfactant concentrations, the viscosities decrease, revealing a partial collapse of the chains, until the viscosity of water is reached.

4. Discussion

4.1. Dynamic Surface Tension. Possible adsorbing species are surfactant monomers (S^+), polyelectrolyte ions (P^-), sodium ions (Na^+), bromide ions (Br^-), and the different kinds of mixed polyelectrolyte/surfactant complexes (i). Making use of the

Gibbs equation, we have

$$d\gamma = -\Gamma_{S^+} d\mu_{S^+} - \Gamma_{P^-} d\mu_{P^-} - \Gamma_{Na^+} d\mu_{Na^+} - \Gamma_{Br^-} d\mu_{Br^-} - \sum_i \Gamma_i d\mu_i \quad (8)$$

where γ is the equilibrium surface tension, Γ the surface excess, and μ the chemical potential of adsorbing species. Sufficiently below the CAC, we could assume that no bulk aggregates are present. Because the surface complex is likely obtained by expelling polymer and surfactant counterions Na^+ and Br^- in the bulk, the third and fourth terms can also be neglected. Doing so accounts for the fact that surface tension is practically independent from bulk polymer concentration³. So below CAC, we are left with the first two terms:

$$d\gamma = -\Gamma_S d\mu_S - \Gamma_P d\mu_P \quad (9)$$

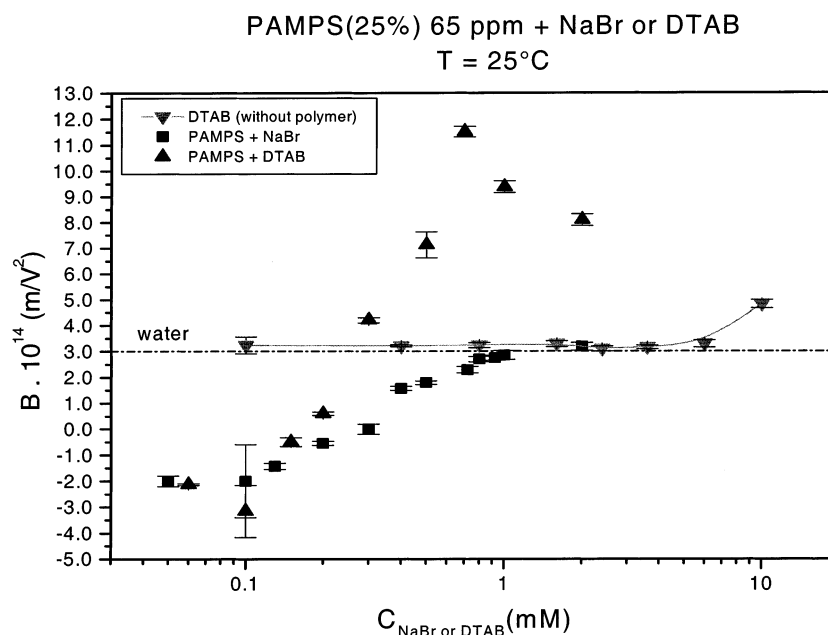


Figure 10. Kerr constant of mixed polymer–surfactant (▲) and polymer–salt (■) solutions versus surfactant or salt concentration for 65 ppm polymer solutions.

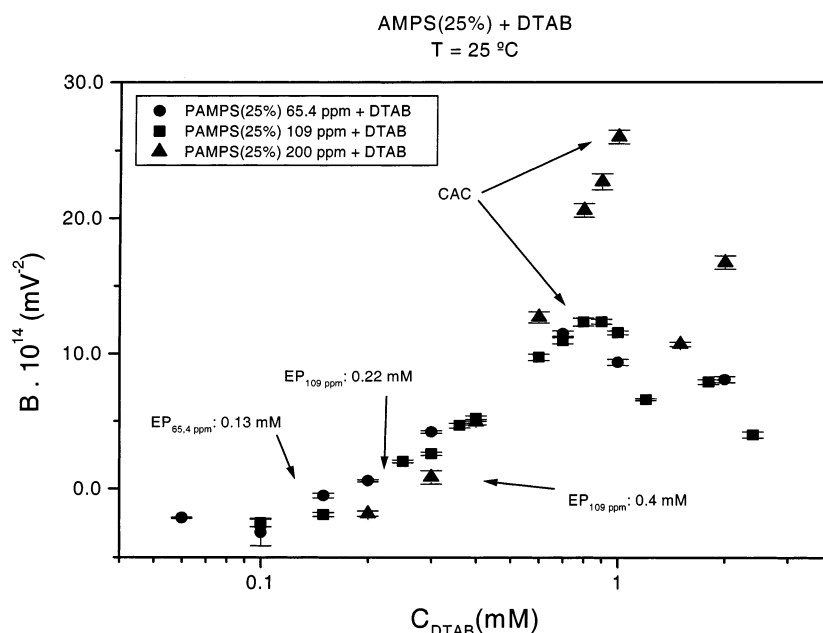


Figure 11. Kerr constant of mixed polymer–surfactant solutions versus surfactant concentration.

Now, at very low concentrations, we can express the chemical potential as

$$\mu_S = \mu_S^0 + RT \ln c_S \quad (10)$$

and then

$$\Gamma_S = \frac{1}{RT} \frac{d\gamma}{d \ln c_S} \quad (11)$$

Strictly speaking, these equations are valid only at equilibrium, so they should be used with caution.

From the equilibrium surface tensions of Figure 3 and eq 11, we get a relatively constant Γ_S ($\Gamma_S = 1.29 \times 10^{18}$ molecules/m²), corresponding to an area per surfactant molecule, $1/\Gamma_S$, of 0.78 nm²/molecule, about twice the area occupied by the

surfactant close to CMC in polymer-free solutions. If we assume that each surfactant molecule at the surface binds one charge of adsorbed polymer molecule, the area per charged monomer will also be on the order of 1 nm²/mol, so the area occupied by the polymer is $1/\Gamma_P \approx 1000$ nm² (there are about 4000 monomers in the chain, 25% of which are charged). This value is consistent with X-ray reflectivity data.^{6,7}

Let us estimate the characteristic adsorption times with the expression¹⁵

$$\tau_i \approx 1/D_i(\Gamma_i/c_i)^2$$

For a surfactant concentration of 0.1 mM and with $D_S \approx 4 \times 10^{-10}$ m²/s, we find $\tau_S \approx 0.1$ s; for a polymer concentration of 100 ppm and with $D_P \approx 10^{-12}$ m²/s (assuming a hydrodynamic

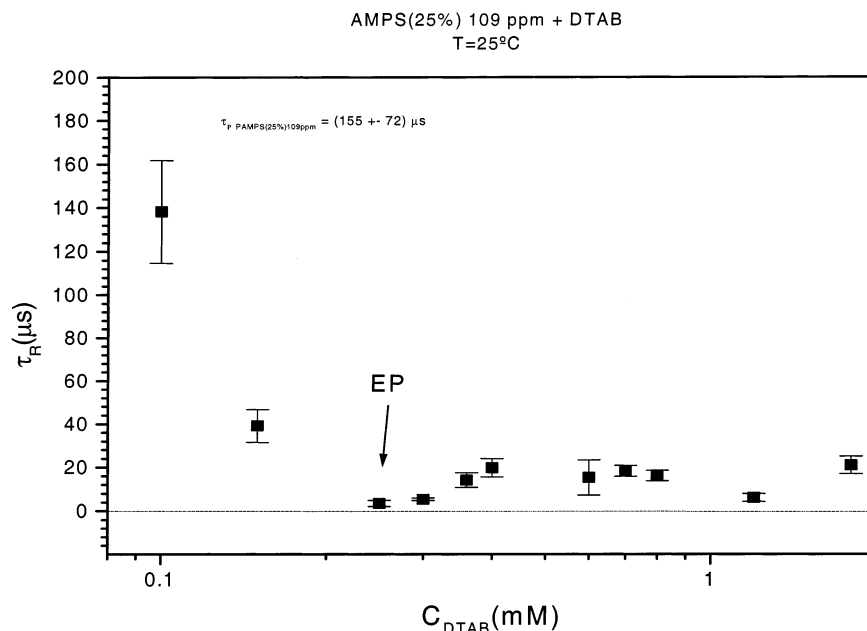


Figure 12. Relaxation time for 109 ppm polymer solutions versus surfactant concentration (data from ref 18).

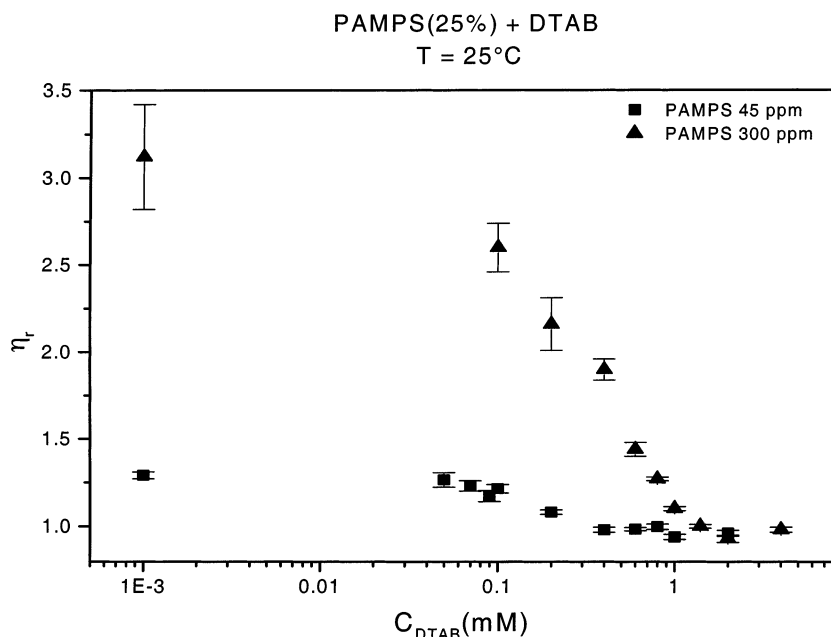


Figure 13. Bulk viscosity versus surfactant concentration for two different polymer solutions.

radius of 100 nm, estimated for an electrostatic persistence length comparable to the Debye length), we find $\tau_P \approx 100$ s. Here characteristic adsorption times are on the order of 1 s; this is longer than surfactant adsorption time but less than polymer adsorption time. It is likely however that the formation of the monolayer involves both species. Indeed, without polymer present, surfactant adsorption is much less. We can then suppose that surfactant adsorption is slowed by the polymer and polymer adsorption accelerated by the surfactant.

4.1.1. Short-Time Adsorption. Following the above discussion, the time region when the surface tension follows a $t^{1/2}$ variation could correspond to the final stage of surfactant adsorption. The slope m is given by

$$m = \frac{RT\Gamma^2}{C_b} \sqrt{\frac{7\pi}{12D}} \quad (12)$$

We see in Figure 6 that m does not depend much on C_P , supporting the assumption that this stage is controlled by surfactant adsorption. The Γ value to be used here is not the equilibrium value. If we use the surface tensions at the break point of the $\gamma(t^{-1/2})$ curves and if we assume that Γ is still given by eq 10, we find a smaller value but again relatively independent of C_S : $\Gamma = 1.6 \times 10^{19}$ molecules/m². The calculated values of D_S below EP are given in Table 1, section a. They decrease with increasing surfactant concentration and become comparable to the polymer diffusion coefficient. So the picture of surfactant adsorption slowed by the polymer seems reasonable.

The net appearance of the plateau on the curves corresponds to the equivalent point for all polymer concentrations. For concentrations above the equivalent point, the adsorption velocity does not continue to increase, suggesting that the free

TABLE 1: Calculated Effective Diffusion Coefficients According to Eq 12 for Solutions Containing 65 ppm PAMPS25%

(a) Short Time Adsorption (Calculation with Surfactant Concentration)		
C_{DTAB} (mM)	m (mN m ⁻¹ s ^{1/2})	D_{eff} (m ² /s)
0.06	0.324	6.78×10^{-11}
0.1	0.37	1.87×10^{-11}
0.15	0.47	5.15×10^{-12}
0.3	0.45	1.41×10^{-12}
0.7	0.46	2.47×10^{-12}
1	0.44	1.32×10^{-13}

(b) Long Time Adsorption (Calculation with Polymer Concentration)		
C_{DTAB} (mM)	m (mN m ⁻¹ s ^{1/2})	D_{eff} (m ² /s)
0.06	9.8	3.99×10^{-17}
0.1	18.6	1.11×10^{-17}
0.15	30.3	4.17×10^{-18}
0.3	48.7	1.61×10^{-18}
0.7	70.2	7.77×10^{-19}
1	72.5	7.28×10^{-19}

surfactant concentration becomes constant, in agreement with the binding isotherm measurements.⁴

4.1.2. Long-Time Adsorption. Let us assume that this stage is controlled by polymer adsorption. From eq 12, one sees that m should be inversely proportional to polymer concentration, in qualitative agreement with the experimental data (Figure 6). At constant polymer concentration, m increases with surfactant concentration, meaning according to eq 12 that the diffusion coefficient decreases because the surface coverage is roughly constant. Above CAC, m remains constant, independent of both C_P and C_S , possibly because at this stage the polymer starts to form bulk aggregates, leaving the free polymer concentration constant.

The calculated polymer diffusion coefficients below CAC using eq 12 are reported in Table 1, section b. The D_P values are smaller than expected, suggesting the presence of a adsorption barrier, possibly due to charge reversal. When such a barrier is present, it is sometimes suggested that eq 12 can still be used but that D should be replaced by $D e^{-E/(kT)}$, E being the energy barrier.¹⁹ Here $e^{-E/(kT)} \approx 10^{-5}$ – 10^{-6} , thus $E/(kT) \approx 12$ – 14 .

Rigorous treatments have been proposed when the barrier is of electrostatic nature,²⁰ which could be the situation here: when enough polymer is adsorbed, charge reversal could occur and lead to a slowing in the late adsorption stages. The plateaus observed above EP (Figure 4b) are in favor of this interpretation. However, it must be pointed out that theory predicts a linear variation of γ with time, instead of the $t^{-1/2}$ variation observed here. We have also checked whether the long-time data could be fitted with exponentials as for reorganization processes in the surface layers,²¹ but the fits with the data were poor. So it seems that the last adsorption stage is truly diffusion-controlled.

4.2. Surface Elasticity. For soluble surfactants, the dependence of surface viscoelastic coefficients on the surfactant concentration for a sinusoidal compression/expansion can be explained by the Lucassen model.²² In this model, it is assumed that upon monolayer compression some surfactant molecules dissolve into the underlying water to restore the equilibrium surface concentration. When the monolayer is expanded again, surfactant molecules come back to the surface.

When the frequency of the oscillating compression is low, the monolayer has always time to reach equilibrium and $\epsilon_r = \epsilon_i$

= 0. When the frequency is high, the monolayer has no time to respond and it behaves as if it were insoluble, $\epsilon_i = 0$ and

$$\epsilon_r = \epsilon_0 = A \frac{\partial \gamma}{\partial A} = -\Gamma \frac{\partial \gamma}{\partial \Gamma} \quad (13)$$

In the intermediate frequency range,

$$\epsilon_r = \epsilon_0 = \frac{1 + \Omega}{1 + 2\Omega + 2\Omega^2}$$

$$\epsilon_i = \omega \kappa = \epsilon_0 \frac{\Omega}{1 + 2\Omega + 2\Omega^2} \quad (14)$$

with

$$\Omega = \frac{D}{2\omega} \sqrt{\frac{\partial C}{\partial \Gamma}}$$

Here, the frequencies used are small, Ω is large, and at least for the surfactant, the soluble regime should be observed. However, because of the presence of the polymer, once adsorbed, the mixed layer behaves as insoluble.⁷ The maximum around CAC means therefore that the monolayer is denser at these concentrations. This has been confirmed by an experiment in which the compressed monolayers are observed simultaneously with a Brewster angle microscope.²³ The fact that ϵ_i is nonzero could be associated with a relaxation process in the monolayer.

4.3. Kerr Effect. As far as we know, there are no quantitative theoretical predictions for the static Kerr effect in the case of flexible polyelectrolyte aqueous solutions^{10,11} that can be accurately compared with the experimental birefringence data. The problem becomes even more complicated because of the surfactant addition. So we only present a qualitative description of the investigated process.

Generally, the Kerr constant, B , in dispersions of particles is proportional to the particle volume (size) and to its anisotropy: *the greater the size and the anisotropy of the particle the greater the Kerr constant.* In the case of a polymer dispersion, a negative sign of the birefringence is generally attributed to the fact that the electric dipoles are perpendicular to the main chain. Here, we are dealing with polyelectrolytes; when salt is added, the polymer charges are screened, meaning that the dipoles perpendicular to the polymer chain vanish progressively. This is probably why the Kerr constant decreases in absolute value when the polymer concentration increases (Figure 9a). The Kerr constant drops to the water value when salt is added (Figure 11a), confirming this picture.

The relaxation time of particles is related to a rotational diffusion coefficient by¹¹

$$D_r = \frac{1}{6\tau_R} \quad (15)$$

and D_r is related to a particle length L by

$$D_r = \frac{3kT}{\pi\eta L^3} [\ln p - 0.76 + 7.5(1/\ln 2p - 0.27)^2] \quad (16)$$

where η is the solvent viscosity and p is the axial ratio.

This simple picture cannot unfortunately apply to polyelectrolyte chains, which are flexible and interact strongly with each other, especially in the semidilute regime. However, we have tried to estimate L from the data. We show the results in Figure 14. The apparent size should be close to the real size

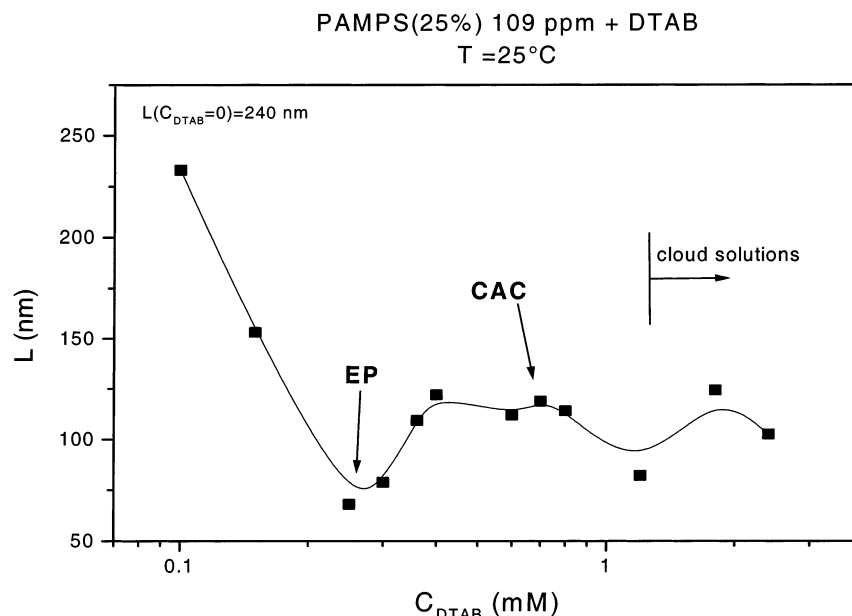


Figure 14. Effective polymer chain length versus surfactant concentration calculated with $p = 100$.

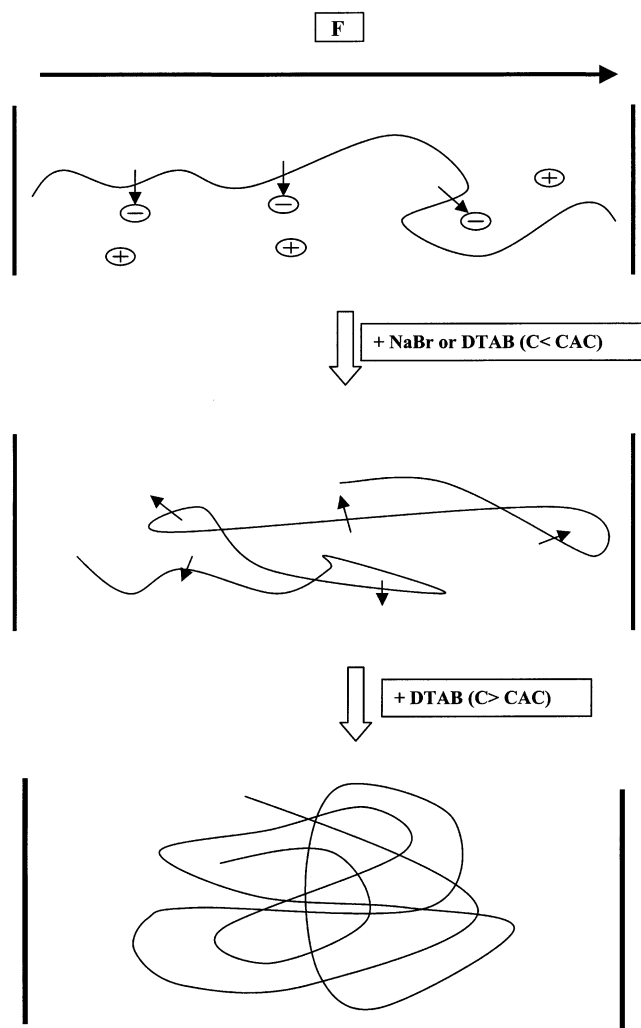


Figure 15. Schematic representation of the polymer-chain conformations.

close to 1 mM DTAB at which the viscosity of the solution is close to that of water (Figure 12) and the polymer chains are partially collapsed and no longer overlapping. At this concentration, the Debye length is around 10 nm, and if we assume that

the persistence length is comparable, with a monomer size of 0.25 nm, we find a total length of 100 nm, comparable to those of Figure 14. It seems therefore that the degree of collapse of the polymer is very limited. This is in agreement with recent quasielastic light scattering experiments²⁴

It should be pointed out that there is a large range of salt concentrations (between 0.2 and 0.8 mM) at which the transient signals are difficult to analyze (they are the combination of positive and negative contributions with different relaxation times). The same effect is seen with surfactant below the EP, although here the transient signals can be fitted with single- or two-exponential curves.

Above EP, the birefringence changes sign. This could be due to the beginning of local association with surfactant chains as depicted in Figure 15. The binding isotherm shows indeed the beginning of a significant degree of association between the polymer and the surfactant.⁴ However, even an association limited to overlap points, either on a single chain or on two adjacent ones (in the semidilute regime), might be sufficient to cause a significant change of the Kerr constant. The decrease of the Kerr constant at DTAB concentrations above CAC could be attributed to an evolution of the conformation of the polyelectrolyte chains toward a more spherical conformation eventually produced by surfactant micelles forming along the chain. This will be consistent with the break point of the surface tension curve of Figure 3.

Conclusion

This study shows the importance of the point of equivalence of charges, both in the bulk and in the surface, of mixed polyelectrolyte–surfactant solutions. Surprisingly the maximum of turbidity or the precipitation does not occur in these systems at the EP, as in simpler mixtures of surfactants of opposite electrical charges.²⁵ However, it is apparent from this work that both adsorption at the surface and interactions in the bulk change above the EP. At the surface, an adsorption barrier, possibly due to charge reversal, starts to build up. In the bulk, the surfactant not only screens the polymer charges but is likely to start binding at the polymer chains. In the systems studied, EP occurs before CAC, as inferred from surface tension curves. More work is clearly needed to understand better the formation

of polymer–surfactant complexes and to be able to model more completely this complex behavior.

Acknowledgment. We are very grateful to Jean-Francois Argillier from Institut Francais du Pétrole for providing purified samples of PAMPS. We also thank Nirmesh Jain for communicating his results to us prior to publication. This work has been supported in part by a cooperation action between France and Argentina, ECOS No. A98E04.

References and Notes

- (1) Goddard, E. D.; Ananthapadmanabhan, K. P. *Interaction of Surfactants With Polymers and Proteins*; CRC Press: Boca Raton, FL, 1993.
- (2) Kwak, J. C. T. *Polymer-Surfactant Systems*; Marcel Dekker: New York, 1998.
- (3) Asnacios, A.; Langevin, D.; Argillier, J. F. *Macromolecules* **1996**, *29*, 7412.
- (4) Jain, N.; Letellier, P. Unpublished data.
- (5) Asnacios, A.; Langevin, D.; Argillier, J. F. *Eur. Phys. J. B* **1998**, *5*, 905.
- (6) Stubenrauch, C.; Albouy, P. A.; Klitzing, R. v.; Langevin, D. *Langmuir* **2000**, *16*, 3206.
- (7) Ritacco, H.; Albouy, P. A.; Bhattacharyya, A.; Langevin, D. *Phys. Chem. Chem. Phys.* **2000**, *2*, 5243.
- (8) Bhattacharyya, A.; Monroy, F.; Langevin, D.; Argillier, J. F. *Langmuir* **2000**, *16*, 8727.
- (9) Guillot, A.; McLoughlin, D.; Jain, N.; Langevin, D. *J. Phys.: Condens. Matter* **2003**, *15*, S219.
- (10) Vijmenga, S. S.; Mandel, M. J. *Mol. Liq.* **1987**, *36*, 119; *J. Chem. Soc., Faraday Trans. 1* **1988**, *84*, 2483.
- (11) Krämer, U.; Hoffmann, H. *Macromolecules* **1991**, *24*, 256.
- (12) Essafi, W.; Lafuma, F.; Williams, C. *Eur. Phys. J. B* **1999**, *9*, 261.
- (13) Miller, R.; Kretzschmar, K. *Adv. Colloid Interface Sci.* **1991**, *37*, 91.
- (14) MacLeod, C. A.; Radke, C. J. *J. Colloid Interface Sci.* **1993**, *160*, 435.
- (15) Fang, J. P.; Joos, P. *Colloids Surf.* **1992**, *65*, 113.
- (16) Lucassen-Reynders, E. H.; Cagna, A.; Lucassen, J. *Colloids Surf., A* **2001**, *186*, 63.
- (17) Ritacco, H.; Kurlat, D. H. *Colloids Surf. A* **2003**, *218*, 27.
- (18) Ritacco, H.; Acosta, E.; Bisceglia, M.; Kurlat, D. *Phys. Chem. Liq.* **2001**, *40*.
- (19) Liggieri, L.; Ravera, F.; Passerone, A. *Colloids Surf., A* **1996**, *114*, 351.
- (20) Diamant, H.; Andelman, D. *Phys. Rev. E* **2000**, *61*, 6740.
- (21) Serrien, G.; Geeraerts, G.; Ghosh, L.; Joos, P. *Colloids Surf.* **1992**, *68*, 219.
- (22) Lucassen, J.; van den Tempel, M. *Chem. Eng. Sci.* **1972**, *271*, 1238; *J. Colloid Interface Sci.* **1972**, *41*, 491.
- (23) Jain, N.; Albouy, P. A.; Langevin, D. *Langmuir*, in press.
- (24) Jain, N.; Delsanti, M. Unpublished data.
- (25) Kaler, E. W.; Murthy, A. K.; Rodriguez, B.; Zasadzinski, J. A. N. *Science* **1989**, *245*, 1371.